https://doi.org/10.5194/egusphere-2023-2538
Preprint. Discussion started: 14 December 2023

Contribution of physical processes to variability of dissolved silicate in the Labrador Sea between 1980 and 2015

Alizée Dale[1], Marion Gehlen[1], Douglas W. R. Wallace[2], Germain Bénard[1], Christian Éthé[1], Elena Alekseenko[3]

[1]Université Paris-Saclay, CNRS, CEA, UVSQ, Laboratoire des sciences du climat et de l'environnement, 91191, Gif-sur-Yvette, France
[2]Department of Oceanography, Dalhousie University, Halifax, Nova Scotia, B3H 1N4 Canada
[3]Laboratoire d'Océanologie et de Géosciences, CNRS, LOG UMR 8187, 28 Avenue Foch, BP 80, 62930 Wimereux, France

Correspondence to: Alizée Dale (alizee.dale@lsce.ipsl.fr)

Abstract. We use output of an eddy-permitting biogeochemical ocean general circulation model to investigate the drivers of the observed decline in the pre-bloom inventory of dissolved silicate (DSi) and its InterAnnual Variability (IAV) over the period 1980-2015. Specifically, the relative impacts of an abrupt decrease in Deep Winter Convection (DWC) and changes in Arctic inflow on DSi concentrations at the regional scale are examined. The IAV of the upper layer DSi inventory covaries with both the Arctic inflow and DWC, however, the pre-bloom decline seems driven primarily by the DWC and associated winter vertical mixing, while the contribution of Arctic inflow is negligible. Our study suggests that the inventory responds to natural decadal variability which is influenced by two major climate modes, the North Atlantic and the Arctic Oscillations, with the former appearing to be the main control.

1 Introduction

The Labrador Sea is a highly productive region within the Subpolar Gyre (SPG; (Harrison et al., 2013; Harrison & Li, 2008), delimited by strong boundary currents (Lazier et al., 2002). Its particularity lies in the intense and variable deep convection which takes place at its center (Lazier et al., 2002; Yashayaev & Loder, 2016). In the central Labrador Sea, the Net Primary Production (NPP) is maintained by deep winter convection (Harrison & Li, 2008; Harrison et al., 2013; Yashayaev & Loder, 2016), which modulates nutrient fluxes, enriching the euphotic layer through vertical mixing (Harrison & Li, 2008; Harrison et al., 2013; Yashayaev & Loder, 2016). Whereas Arctic Inflow modulates NPP on the Labrador (Tremblay et al., 2015) and Greenland shelves (Tesdal et al., 2022). In the Labrador Sea, NPP is mainly supported by diatoms (60 to 80%; Rousseaux & Gregg, 2013). Diatom productivity is at the base of a productive food chain that supports higher trophic levels (Conti &

https://doi.org/10.5194/egusphere-2023-2538
Preprint. Discussion started: 14 December 2023

Scardi, 2010; Stock et al., 2017) including valuable fisheries, among others, of Atlantic salmon, cod, mackerel, and herring (Government of Canada, Fisheries and Oceans Canada, Communications Branch, 2021).

In contrast to other phytoplankton groups which are dependent on light, nitrogen, phosphorus and iron to grow, diatoms also require dissolved silicic acid or silicate ($Si(OH)_4$, referred to here as DSi) to form their frustules (Egge & Aksnes, 1992; Nelson & Dortch, 1996). DSi concentrations showed a negative trend between the mid-1990s and the late 2000s (Hátún et al., 2017; Tesdal et al., 2022). Even though the trend appeared to reverse starting from the 2010s (Tesdal et al., 2022), the decrease of DSi concentrations was reminiscent of a regime shift. This regime shift may reflect projected future conditions, which are typically characterized by a weakening of the winter-time deep convection and a slowdown in circulation (Lenton et al., 2008; McKay et al., 2022). Variability of winter-time deep convection appears similar to that of DSi concentration. It weakened abruptly from 1994 onwards, shoaling from a MLD of 1000-2400 m between 1987 and 1994, to roughly 1000 m between 1994 and the early 2000s (Lazier et al., 2002; Yashayaev & Loder, 2016), while intense events reoccured between 2014 and 2015 (Yashayaev & Loder, 2016). During the same period, a slowdown in the SPG circulation was observed (Hakkinen & Rhines, 2004; Hátún et al., 2005; Hátún et al., 2017; Tesdal et al., 2022). The weakening of the SPG led to unbalanced mixing between DSi-Rich Arctic Waters (SRAW) and a greater volume of DSi-poor waters from the south compared with the period preceding the SPG weakening (Hátún et al., 2017). This imbalance led to water that was poorer in DSi, reaching the Labrador Sea through the SPG circulation following the Greenland continental margin (Tesdal et al., 2022). From the Arctic, the SRAW transport is also supposed to have weakened from the mid-1990s (Aksenov et al., 2016), leading to negative anomalies in DSi concentrations along their transport pathways (Tremblay, 2002; Hátún et al., 2017) compared to the early 1990s.

The relative importance of the contribution of advective fluxes from the Arctic, from the SPG circulation and from winter-time deep convection to the observed variability of DSi concentration has been debated (Harrison & Li, 2008; Hátún et al., 2017; McKinley et al., 2018; Tesdal et al., 2022). Such a decrease in DSi, and the potential for future regime shifts, could have significant consequences for NPP, ranging from a reduction in primary production to changes in phytoplankton community composition (and, potentially, sinking fluxes) due to a reduction in diatom biomass.

Here, we draw on output from an eddy-permitting ocean general circulation biogeochemical hindcast simulation to examine and quantify the relative contributions of an abrupt decrease in winter-time deep convection and changes in Arctic inflow to the variability of DSi concentrations at the scale of the Labrador Sea. Finally, we briefly put the decline in DSi into perspective with changes in net primary production (NPP).

In Section 2, we describe the model set-up and analysis methods. In Section 3, we focus on the influence of the DSi decline on NPP, and compare the DSi decline in the model to observations along a hydrographic section. We quantify the contribution of Arctic Inflow to the variability of DSi inventory. The use of two metrics, annual maximum MLD and DSi fluxes at the base of the mixed layer induced by vertical mixing, allows us to identify deep convection as the main contributor to the strong decrease of DSi during the 1990s. Finally, we discuss the link between weather regimes and

https://doi.org/10.5194/egusphere-2023-2538
Preprint. Discussion started: 14 December 2023

variability of DSi concentrations in relation to the physical forcing factors under investigation, and associated future ecosystem impacts.

2 Material and methods

The study focuses on the area delimited by two sections to the north and south of the Labrador Sea (Fig. 1). To account for mass transport through Hudson Strait, the northern limit is defined by a section located just to the south of Davis Strait. We refer to this as the Northern section in the remainder of the paper. The Labrador Sea is closed to the south by the OSNAP-West section (Fig. 1.a). To address the variability of DSi available for primary production, our analysis focuses on the upper layer of the water column between 0 and 450 m depth. This depth criterion (<450 m) corresponds to the shallowest extent of the maximum Mixed Layer Depth (MLD), as simulated by our model within the area of study.

2.1 Observational and numerical datasets

2.1.1 NEMO-PISCES model

The model used to evaluate physical contributions to the variability of the DSi inventory within the Labrador Sea is based on a global configuration of the Nucleus for European Modelling of the Ocean (NEMO; stable 3.6 version; Madec et al., 2017). The extended version of the tripolar grid eORCA has a resolution of 0.25° in longitude and 0.25° cosϕ in latitude (eORCA025). There are 75 vertical levels with a resolution of 1 to 15 m between the surface and 200 m depth, and of 50 m to 100 m between 500 m and 1000 m depth. The model is forced with the DRAKKAR Forcing Set (DFS) 5.2 (Dussin et al., 2016) for the period 1958 to 2015 under constant pre-industrial atmospheric CO_2 (284.32 ppm). The ocean general circulation model is coupled online to the Louvain-la-Neuve sea-ice model LIM3 (Vancoppenolle et al., 2009) and the Pelagic Interaction Scheme for Carbon and Ecosystem Studies (PISCES-v2; Aumont et al., 2015). PISCES is a biogeochemical model which describes the lower trophic levels of the marine food web with four plankton functional types: diatoms and nanophytoplankton, as well as micro- and meso-zooplankton. Phytoplankton growth is co-limited by 5 nutrients (iron, phosphate, nitrate, ammonium and dissolved silicic acid), light, and modulated by temperature. The model has been initialized with observation-based climatologies listed in table S3 and with external nutrient sources listed in table S4 of the supplementary material (section 2).

https://doi.org/10.5194/egusphere-2023-2538
Preprint. Discussion started: 14 December 2023

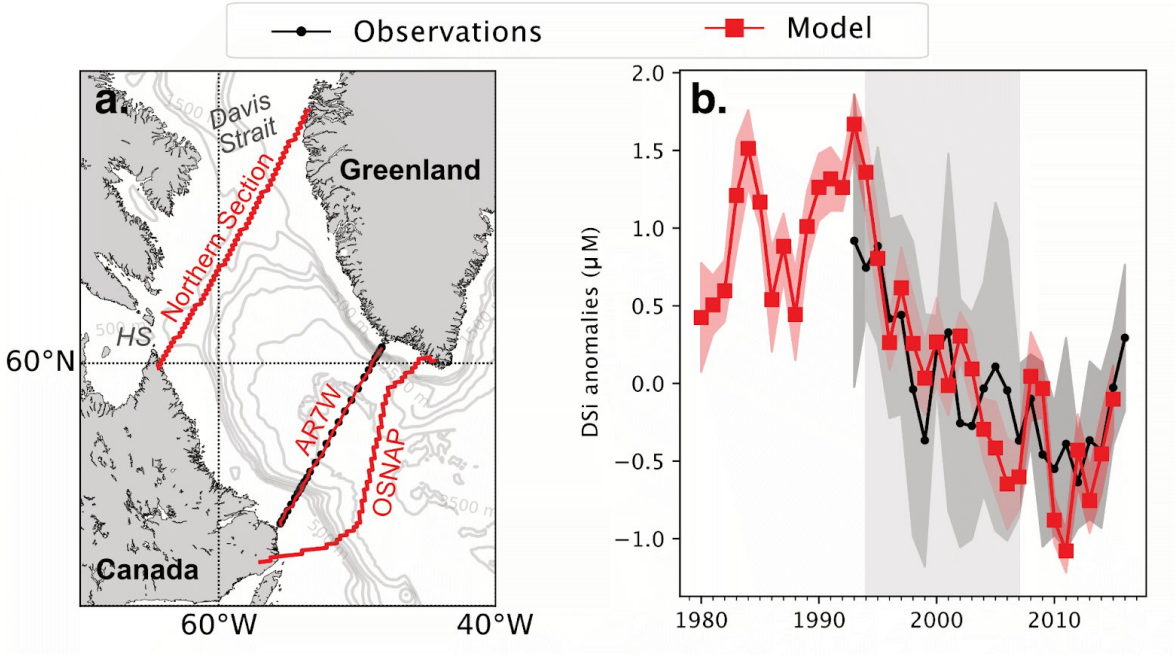

Figure 1: Observed (black) and simulated (red) anomalies of the DSi concentration along the AR7W section in spring (April, May, June) relative to the mean over the 1993-2015 period for the upper (0-450 m) layer. (a) The region of study is delimited by the OSNAP-west section to the south and a Northern section south of Hudson Strait (HS) and Davis Strait. Model grid points that constitute the sections are shown in red. The DSi concentration profiles measured along the AR7W section are shown in black. (b) The solid line shows average DSi concentrations anomalies (0-450 m) along the AR7W section from the model (red) and observations (black). Red shaded areas represent the standard deviation of monthly concentration anomalies in the model. The dark grey shading indicates the standard deviation of observed concentration anomalies along the whole section.

In this study, we consider the following variables: dissolved silicate (DSi), conservative temperature, practical salinity, effective transport, Mixed Layer Depth (MLD; defined by a density difference of 0.01 kg/m^3 relative to water at 10 m depth), and Sea Level Pressure from the atmospheric forcing dataset (DFS5.2). The simulation starts from an ocean at rest in 1958. We limited our analysis to the period 1980-2015, i.e., the period from which the integrated volume between OSNAP and the Northern section reached a quasi steady-state (Fig. S1).

2.1.2 Observational dataset

This study draws on several observational data sets for the evaluation of mean state and interannual variability of modeled properties. Units were converted as needed. Details of model evaluation are presented in the supplementary material. Modeled temperature and salinity were compared along Davis Strait to data from the 2004 R/V Knorr cruise

https://doi.org/10.5194/egusphere-2023-2538
Preprint. Discussion started: 14 December 2023

(https://cchdo.ucsd.edu/cruise/316N20040922). Simulated mixed layer depths were evaluated over the 1980-2017 period against observation-based estimates derived from a combination of Argo and CTD data across the Labrador Sea and processed at the Bedford Institute of Oceanography (Yashayaev & Loder, 2016; Raimondi et al., 2021). Modeled mean states of temperature, salinity, DSi, and MLD over the full area of study and 1981-2010 were compared to corresponding averages computed from the World Ocean Atlas 2018 Reanalysis (https://www.ncei.noaa.gov/).

Interpolated data from the Atlantic Repeat Hydrography Line 7 West (i.e., AR7W, from GO-SHIP, WOCE, and CLIVAR cruises supported by Canada's Atlantic Zone Offshore Monitoring Program) were used to evaluate the modeled variability of DSi. This section lies between the OSNAP, and Northern sections and data are available from 1992 to 2015 (https://cchdo.ucsd.edu). Note that DSi concentrations were mainly measured in spring or summer and that we used only the average concentrations between 0 and 450 m in this study.

2.2 Methods

2.2.1 Spring bloom NPP

Total monthly NPP has been integrated from top to bottom and between April and June (the months in which the spring bloom occurs), in order to describe NPP conditions preceding and following the trend in DSi concentration. The bloom initiation is determined following Siegel et al (2002) as the time at which NPP exceeds its yearly median by 5%. The threshold is relative to the spring bloom of a given year, thus eliminating the effects of inter-annual variability.

2.2.2 Pre-bloom DSi inventory

The variability of DSi is represented by its average pre-bloom inventory (March-April average) as a measure of its potential to limit annual primary production. The pre-bloom DSi inventory is calculated from an integration of pre-bloom DSi concentrations (µM) of each grid cell within the entire volume of the upper layer (0-450 m) between the OSNAP and Northern sections, multiplied by the volume of the associated grid cell. The inventories are given in teramoles (Tmol) of DSi.

2.2.3 Contribution of the Arctic inflow

The annual average DSi import by transport across the Northern Section is given in Tmol and calculated by integration of the monthly DSi transports (in kmol/s). The variability of DSi transport is assessed with reference to its annual average (1980-2015).

https://doi.org/10.5194/egusphere-2023-2538
Preprint. Discussion started: 14 December 2023

In the model, net volume transport (TRP) and net DSi transport (TRP_{DSi}) are calculated from the meridional and zonal components of effective transport (T_{eff}), following Eq. (1) and (2). The effective transport is derived from the sum of the Eulerian velocity and the eddy-induced velocity diagnosed during the simulation at the model time step for each grid cell.

$$TRP = \int_{west}^{east} \int_{0}^{h=450m} T_{eff}\,(x,y,z)\,dz\,dx,y \quad (1)$$

$$TRP_{DSi} = \int_{west}^{east} \int_{0}^{h=450m} T_{eff}\,(x,y,z) \times \left[\overline{DSi}\right](x,y,z)\,dz\,dx,y \quad (2)$$

where [*D*Si] is the average nutrient concentration at the center of the two grid cells surrounding the T_{eff} grid point (details in section 2.1 of the supplementary material). T_{eff} is located on the edges of the cells at point U or V (Fig. S7) on the type-C Arakawa grid (Mesinger and Arakawa, 1976). z is the depth coordinate, and x, y are the zonal and meridional coordinates of the section. Hydrographic sections have been co-localized on the model grid to select the suitable component of T_{eff} and to associate it with the appropriate mean concentration. Note that by convention, southward transports are negative and northward transports are positive.

2.2.4 Contribution of deep winter convection

To assess the contribution of deep winter convection, we evaluated (i) the temporal evolution of the Mixed Layer Depth (MLD), and (ii) the net exchanges of DSi at the base of the Mixed Layer (ML). The latter allows quantification of the variability of DSi import into the ML by vertical mixing processes (Eq. (3)), i.e. entrainment or detrainment of DSi at the ML base (positive sign for detrainment and negative for entrainment to the ML) and the contribution of vertical diffusion of DSi across the ML base. These terms were computed during the simulation and, at the time step of the physical model. In order to compare the contribution of import by vertical mixing to the variability of the DSi inventory, it has been converted from kmol/s to an annual amount (Tmol of DSi) as was done with the DSi transport across the Northern section.

$$Vertical\ mixing = \underbrace{(k_z \partial_z [DSi]_{mld}}_{Vertical\ diffusion} - \underbrace{[DSi]_{mld} \cdot \partial_t mld}_{Entrainment/Detrainment} \quad (3)$$

In Eq. 3, k_z is the vertical diffusion coefficient at the mixed-layer base whose minimal value is 10^{-5} m^2/s, *mld* is the depth at the ML base and $[DSi]_{mld}$ is the DSi concentration at the ML base.

2.2.4 Climate Indices

The region of study is under the influence of two weather regimes that influence the atmospheric forcing (i.e., winds, surface air temperature) above the North Atlantic: the North Atlantic Oscillation (NAO) and the Arctic Oscillation (AO).

https://doi.org/10.5194/egusphere-2023-2538
Preprint. Discussion started: 14 December 2023

The NAO is characterized by a redistribution of atmospheric mass between the Arctic and subtropical Atlantic (Hurrel et al. 2003). It is an oscillation that represents a pressure gradient between the Azores high-pressure and the Iceland low-pressure, between which flow the westerlies. Since the intensity of these winds may increase or decrease the heat loss from the Labrador Sea (Bersh et al., 2007; Lohmann et al., 2009; Hakkinen et al., 2011), we calculated the NAO index to quantify the variability of this oscillation and relate it to the observed trends in DSi concentration. The NAO index is based on an Empirical Orthogonal Function (EOF) analysis of the Sea Level Pressure (SLP in Pa; Hurrel et al., 2003) over the domain 30°N-80°N, 85°W-30°E. SLP comes from the DFS5.2, which forced the model with ERA-interim reanalysis. For the EOF analysis, we use the winter mean (DJF) of the SLP over the 1979-2015 period. The result shows a first mode representing 26.9 \% of the SLP variability and a South-North dipole.

A similar method is used to quantify the AO. The AO is described as a pattern of SLP centered on the Arctic (Thompson et al., 1998; Hamouda et al., 2021) . To track its variability, it is defined by an index calculated from the principal component of an EOF analysis of the winter mean SLP (DJF) above 20°N (Thompson et al., 1998; Hamouda et al., 2021).

3 Results

3.1 Observed and simulated DSi variability

A Labrador Sea-wide evaluation of simulated temperature, salinity, MLD and DSi concentration against observation-based datasets is reported in the supplementary material (section 1.2) along with a synthesis of data sets (Table S1). Overall, the model overestimates surface DSi concentrations on the eastern side of the Labrador Sea (i.e., on the Greenland continental margin) whereas they are underestimated at the surface on the western side of the Labrador Sea (i.e., on the Canadian continental margin). DSi concentrations below the surface, and over the full upper layer (0-450 m) are underestimated throughout the basin. The temporal evolution of average DSi concentrations in the model and measured along the AR7W section (Fig. 1a), are shown in Fig. 1.b, where concentrations are presented as anomalies relative to the average over the period 1993-2015. The model underestimates observed concentrations by 2.3 µM on average (Fig. S5). Despite this bias, the phasing and amplitude of DSi interannual variability are well reproduced, with a strong, significant correlation between the observed and modeled decline (1994 to 2007: Pearson's R = 0.71, p-value < 0.01, Fig. S5b).

The period of DSi decline (Fig. 1b), between 1994 and 2007, is surrounded by a) a first period, between 1980 and 1993, characterized by a higher average concentrations and strong interannual variability; b) a third period, between 2008 and 2015, which is marked by an increase of DSi concentrations. During the period of decline (1994-2007), modeled DSi anomalies decreased linearly at a rate of -0.09 $\mu M.yr^{-1}$ (p-value < 0.01). Observed DSi concentrations displayed a smaller decrease over the same period (-0.05 $\mu M.yr^{-1}$, p-value < 0.01).

https://doi.org/10.5194/egusphere-2023-2538
Preprint. Discussion started: 14 December 2023

3.2 Contribution of the Arctic inflow

Between 1994 and 2007, the pre-bloom DSi inventory and the import of DSi from the Arctic both declined. The negative trend was, however, much larger for the inventory (-0.038 Tmol.yr^{-1}) than for the DSi import (-0.0013 Tmol.yr^{-1}) across the Northern section (Fig.2a). The difference in trends translates into a much larger amplitude of decline of the prebloom inventory (0.66 Tmol) than of the average annual import of DSi from the Arctic (0.02 Tmol). This implies that the reduced influx of DSi across the Northern section is responsible for only about 3% of the inventory decline. On the other hand, time series of DSi transport across the Northern section and of the Labrador Sea DSi inventory show a consistent variability over the entire study period (1980-2015) and are significantly correlated (Pearson's R = 0.88, p-value = 10^{-5}). The former suggests a common driver of variability which is also indicated by the linear relationship between DSi transport and inventory shown in Fig. 2c.

https://doi.org/10.5194/egusphere-2023-2538
Preprint. Discussion started: 14 December 2023

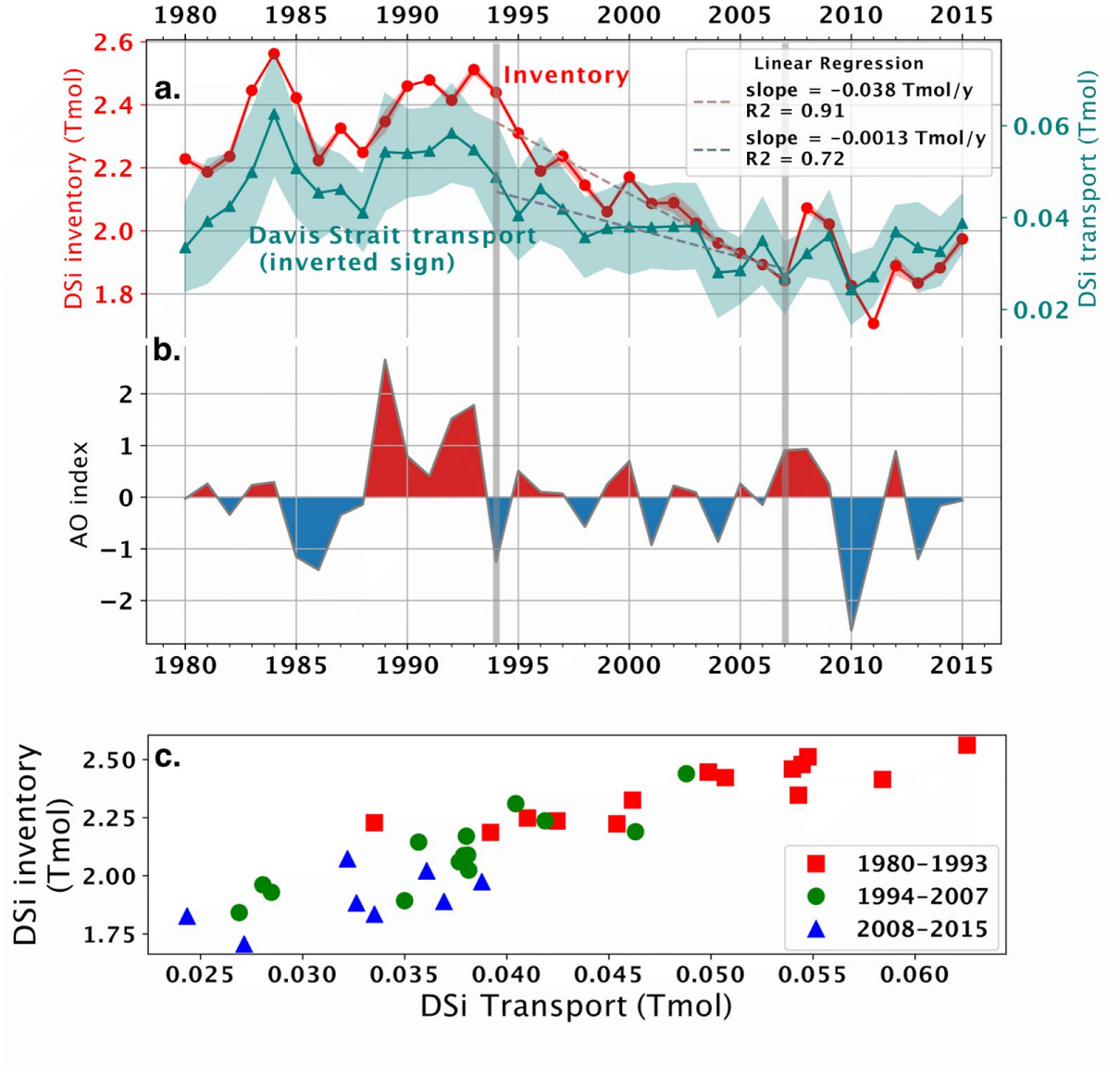

Figure 2. a. Temporal evolution of the upper layer average pre-bloom DSi inventory (in red) and annual average import of DSi from the Arctic inflow across the Northern section upper layer (in blue) between 1980 and 2015. Note that the sign of the DSi transport across the Northern section has been reversed for comparison with the DSi inventory changes. The more positive the transport, the more DSi is transported into the area of study. Standard deviations around the two averages are shown by colored shading. A linear regression model has been computed from 1994 to 2007 for both time series (dashed line, p-value < 0.01). The result of the linear regression is given in the top right corner of the Fig. b. Time-series of the Arctic Oscillation index calculated from an Empirical Orthogonal Function analysis of the Sea Level Pressure for latitudes greater

https://doi.org/10.5194/egusphere-2023-2538
Preprint. Discussion started: 14 December 2023

than 20°N. c. Scatter plot of the pre-bloom DSi inventory and annual average DSi inputs from the Northern section transport (as shown in Fig. a.).

3.3 Contribution of deep winter convection

The annual variations of the pre-bloom inventory also co-vary with estimates of DSi entrained into the mixed layer by deep winter mixing (Fig. 3), particularly before ($r = -0.88$, p-value = 10^{-5}) and during ($r = -0.81$, p-value = 10^{-4}) the period of decline. Due to the shortness of the final period, the same relationship cannot be statistically confirmed but the time series in Fig. 3a is still suggestive of a correlation. The input of DSi from vertical mixing dropped between 1993 and 1996, followed by a roughly linear decline of -0.12 Tmol.yr^{-1} up to 2007 which mirrors the decline in inventory (-0.39 Tmol.yr^{-1}). The amplitude of the decline of the contribution of deep winter mixing is -0.83 Tmol between 1994 and 2007 which is comparable with but somewhat larger than the corresponding reduction of the pre-bloom DSi inventory (-0.66 Tmol). The entrainment of DSi through vertical mixing was calculated at the base of the mixed layer which reaches depths far exceeding 450 m during some years (e.g. 2000 m in 1993). As a result, it is associated with a layer much deeper and richer in DSi than the layer over which the inventory was calculated explaining why its amplitude exceeds that of the inventory (e.g. in 1993, MLD reached 2000 m where the DSI concentration was 11.6 µM, whereas its average concentration varies from 6 µM (in 2007) and 8 µM (between 1990 and 1994 at 450 m) .

In the following, we focus on the annual maximum Mixed Layer Depth (MLD) as a metric to describe the intensity of deep winter convection. The annual maximum MLD corresponds to the maximum depth reached by the ML over the course of a year. The convection zone associated with the renewal of Labrador Sea water is identified based on a critical depth of 1000 m following Rühs et al. (2021). Figure 3.c presents the annual maximum MLD averaged over the three periods identified before, as well as the horizontal extent of the associated convection zones. The extent of the convection zone and the depth reached were both greatest between 1980 and 1993, just before the decline in DSi inventory. This was followed by a sharp decrease in the area of the convection zone between 1994 and 2007, associated with shallower MLDs. Between 2008 and 2015, the convection zone expanded again. The histogram (Fig. 3d) displays the depth distribution of the annual maximum MLD within the 1980-2015's average convection zone (black contour in Fig. 3c) for each of the three periods. It confirms the existence of distinct regimes with the first period (in red) being characterized by deep convection depths and clearly distinct from the period of declining DSi (in green). The third period (in blue) could be interpreted as a transition phase towards greater convection depths. Contrary to the DSi transport across the Northern section, which is characterized by an overall linear decline, the reduction of the annual maximum MLD occurs in the model as an abrupt shift towards shallow MLDs over a period of about two years (1993 to 1995).

https://doi.org/10.5194/egusphere-2023-2538
Preprint. Discussion started: 14 December 2023

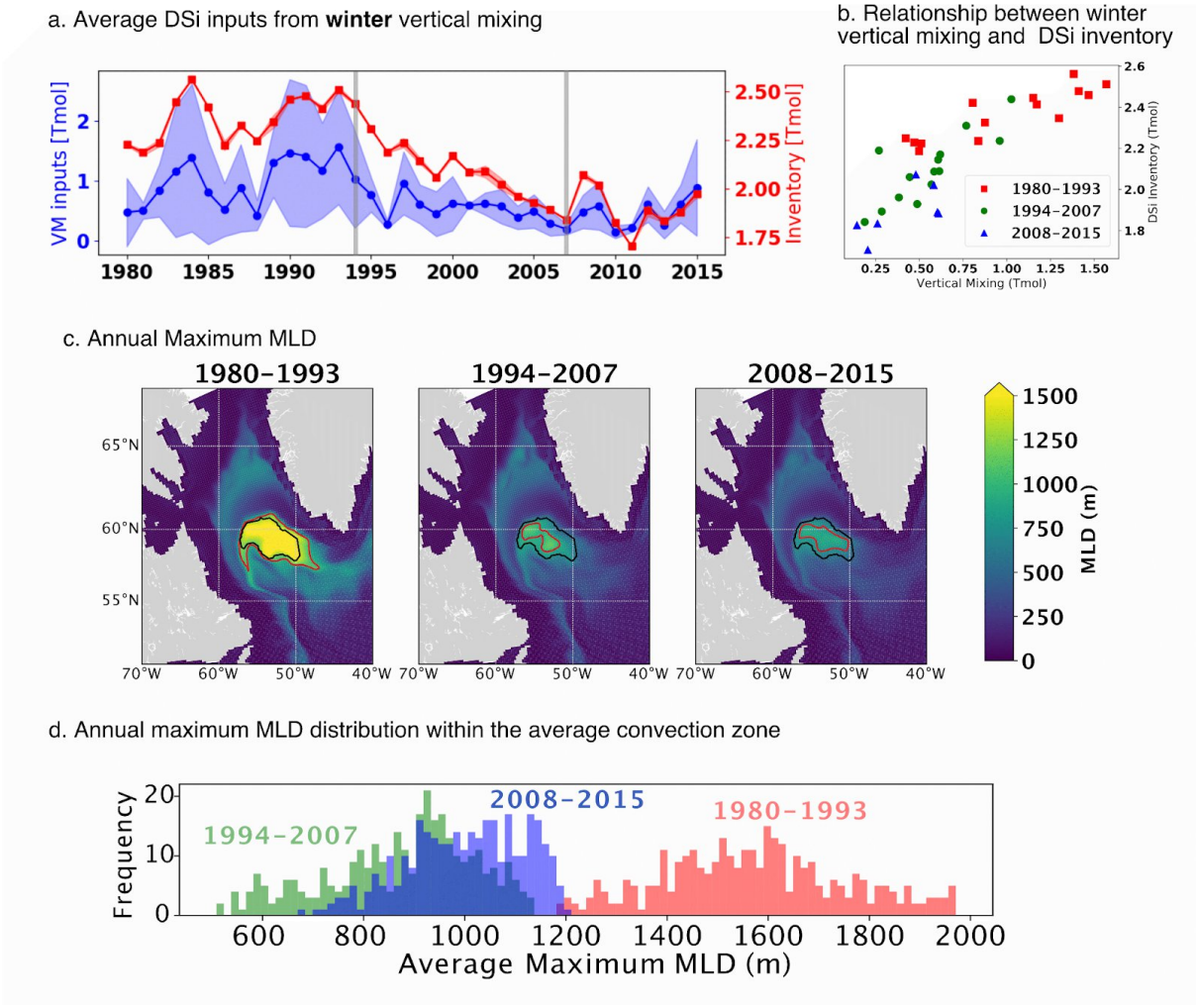

Figure 3. Relationship between winter deep convection and the pre-bloom DSi inventory. (a.) Temporal evolution of average winter DSi inputs from vertical mixing in blue and the average pre-bloom DSi inventory of the upper layer in red. Coloured shading displays the standard deviation. (b.) Relationship between average winter DSi inputs from vertical mixing and the pre-bloom DSi inventory of the upper layer with a focus on the three study periods, which suggests a constant linear relation between these two variables. (c.) Annual Maximum MLD averaged for the three periods. The red contour delimits the convection zone specific to the period under consideration, while the black contour indicates the average convection zone over the entire period (1980-2015). The same critical convection depth as Rühs et al. (2021) of 1000 m has been chosen to define convection zones. Note that MLDs greater than 1500 m are displayed in oversaturated yellow. The associated histogram (d.) represents the depth distribution of the ML at each grid cell within the 1980-2015 average convection zone (black contour), for each period.

https://doi.org/10.5194/egusphere-2023-2538
Preprint. Discussion started: 14 December 2023

3.4 Changes in Net Primary Production

In order to evaluate the impact of the DSi decline on NPP, we compare average total NPP before and after the decline in DSi concentration (Fig. 4a). Prior to the decline in DSi concentrations (i.e. 1980-1993), modeled average total NPP integrated over the months of the spring bloom reached maximum values on the continental shelf of Greenland and Canada (Fig. 4a; between 200 and 240 gC/m2/year). Values were lower in the central basin (between 120 and 160 gC/m2/year). Considering the period following the decline in DSi concentrations, NPP declined over ~69% of the study area between 1980-1993 and 2008-2015 Fig. 4b). Increases in NPP were mostly confined to the eastern to northern slopes of the basin. NPP anomalies for the period 2008-2015 relative to the 1980-1993 period, were modest compared to the average NPP values.

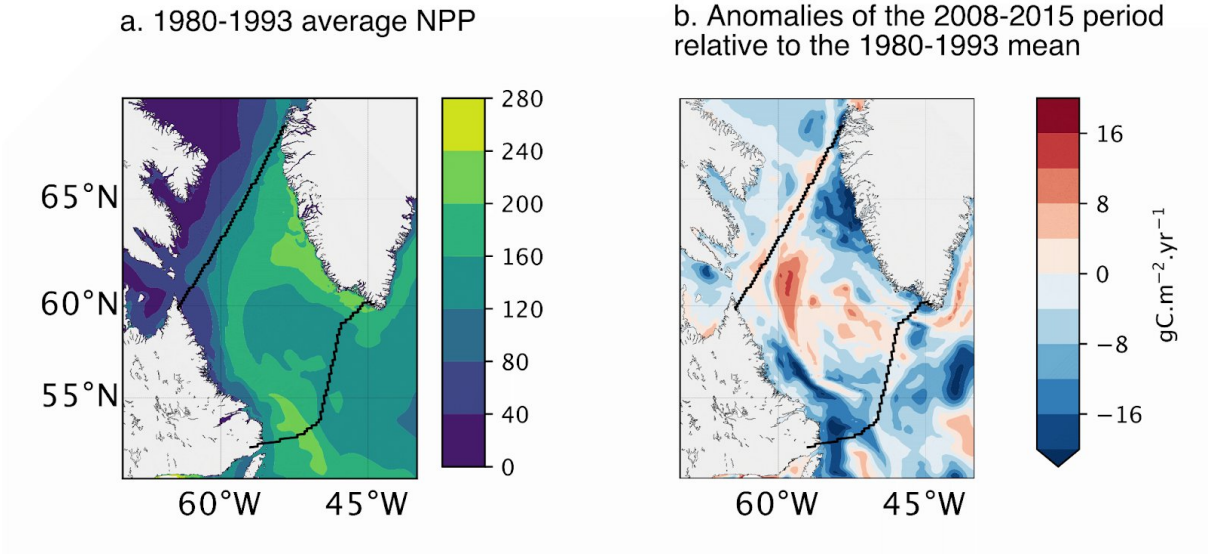

Figure 4. **Evolution of top-to-bottom integrated NPP.** a. Average between 1980 and 1993. b. 2008-2015 NPP anomalies relative to the 1980-1993 mean.

4 Discussion

The present study has highlighted distinct differences in NPP, DSi concentration (and inventory), lateral transport, and MLD in the Labrador Sea between the three time periods from 1980 to 2015. Compared to the first period (i.e., 1980-1993), between 2008 and 2015, the Labrador Sea showed a slightly reduced NPP (i.e., the median reduction is equivalent to -4% of the median NPP where anomalies are negative. Maximum negative anomalies reach -14% of the local average at the point where the reduction is the greatest) in the center of the basin and in the most productive areas of the study region. This reduction coincides with lower DSi concentrations and inventory, a minor reduction in lateral DSi inputs from the North and east, and a major reduction in vertical mixing. The latter relates to shallower winter-time convection. Between these two

https://doi.org/10.5194/egusphere-2023-2538
Preprint. Discussion started: 14 December 2023

periods, from 1994 to 2007, the concentrations and inventory of DSi in the Labrador Sea declined progressively, as did all physical sources of nutrients (i.e., lateral transport and vertical mixing). In the following discussion, we will first address the changes in the Labrador Sea between 1994-2007 and then qualitatively assess the implications of this natural variability in the context of projected future global warming conditions.

4.1 Observed and modeled decline in DSi

The model suggests a linear decrease in DSi concentration between 1990 and 2015 of -0.09 µM/yr , twice as large as the observed trend (-0.04 µM/yr, Hátún et al., 2017; Yeats et al., 2011). This difference can be partly explained by the interannual variability of the modeled DSi concentration, which has a higher amplitude than its measured counterpart. For example, (Fig. 1a) between 1990 and 2015, modeled concentration anomalies along the AR7W section range from (-1.08 ± 0.19) µM in 2011 to (+1.67 ± 0.36) µM in 1993, whereas the anomalies in observations range from (-0.64 ± 0.30) µM in 2012 to (+0.92 ± 0.94) µM in 1993.

The above values are given between 1990 and 2015 for comparison. From observations (Hátún et al., 2017; Tesdal et al., 2022) and the model, it is clear that the DSi decline began in 1994. Coupled with the fact that model outputs stopped in 2015, the reappearance of strong interannual variability from 2007 onwards makes it difficult to identify the end period of the decline and the possibility of a return to 1980-1993 concentrations. However, recent observations (up to 2018) indicate increased DSi concentrations to the level observed before 1994 (Tesdal et al., 2022). Whereas the decline in DSi from 1994-2007 was caused by the abrupt weakening of winter deep convection, the increase surrounding 2015 seems conversely to follow conditions favorable to intense winter deep convection (Yashayaev, 2023).

4.2 Regime shifts in the central Labrador Sea

The model output shows a change in the winter-time deep convection regime between the period 1980-1993 (annual maximum MLD between 1184 and 1970 m) and 1994-2007 (between 508 and 1130 m). This change in regime does not affect the DSi inventory as dramatically, as the DSi inventory shows a linear decrease. The plurality of processes modulating the variability of the DSi inventory, such as boundary currents (i.e. the West Greenland Current and the Labrador current), may be the cause (Tremblay et al., 2015; Tesdal et al., 2022). Similarly, NPP is not affected as strongly by the change in convection regime because of its modulation by other factors (e.g. co-limitation by light and nitrate (not discussed in this paper; Harrison & Li, 2008). Nevertheless, model results suggest a change in phytoplankton community composition to the north of the study area which is marked by an increase in nanophytoplankton biomass and a decrease in diatoms biomass (Fig. 5), the two phytoplankton groups represented by the model. Such a change is consistent with observations of an increase in small phytoplankton and a decrease in large phytoplankton (Harrison & Li, 2008).

https://doi.org/10.5194/egusphere-2023-2538
Preprint. Discussion started: 14 December 2023

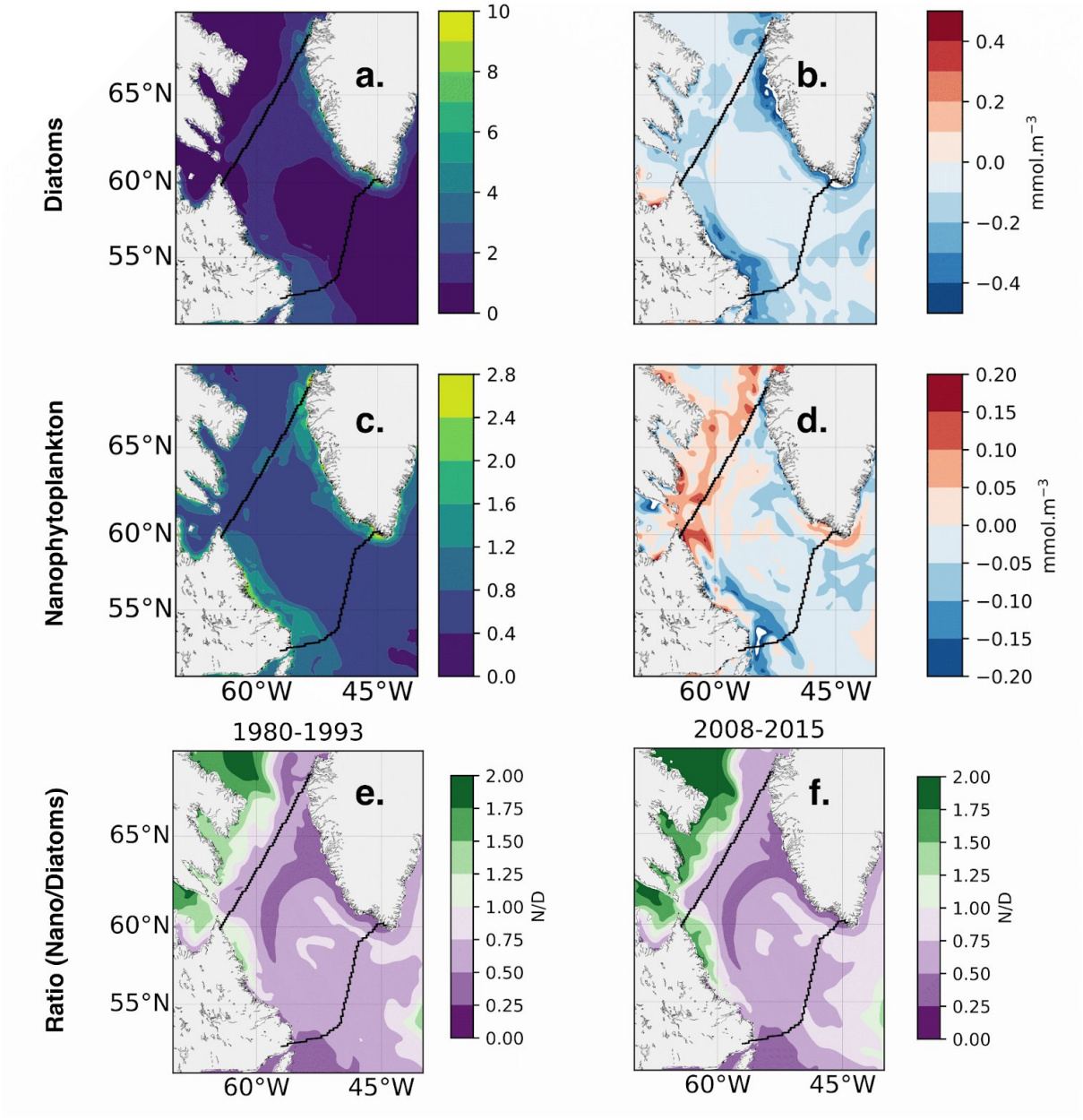

Figure 5. Evolution of top-to-bottom integrated diatoms (top) and nanophytoplankton (bottom) biomasses integrated on spring months (April to June). (a.,c.) Average between 1980 and 1993. (b.,d.) 2008-2015 biomass anomalies relative to the 1980-1993 mean. (e.-f.) Ratio of average nanophytoplankton biomass (N) over biomass diatoms biomass (D) for the period 1980-1993 (e.) and 2008-2015 (f.). Note that purple highlights diatoms-dominated areas and green nanophytoplankton-dominated areas.

https://doi.org/10.5194/egusphere-2023-2538
Preprint. Discussion started: 14 December 2023

4.2 Physical causes of DSi variability

The present study has shown that the contribution of DSi transport from the Arctic is correlated but negligible (= 3%). Our estimate of the Arctic inflow's contribution to DSi's pre-bloom decline falls below the range of 10 to 20% given by Hatun et al. (2017). The difference between the estimates most likely reflects the different approaches taken: direct computation of transport of DSi across a section closing the Labrador Sea to the North (this study) as opposed to an indirect assessment based on an estimation of DSi retention upstream in the Beaufort Gyre. Both estimates, however, suggest a minor to negligible contribution of DSi transport from the Arctic to the decline of its inventory in the Labrador Sea. Although the contribution is negligible at the scale of the study region, Arctic water appears to dominate and locally characterize the water occupying the Labrador Shelf along the Canadian coast (Torres-Valdés et al., 2013; Fragoso et al., 2016). This DSi-rich water (Tremblay, 2002) limits primary production locally (Fragoso et al., 2016).

More broadly, DSi concentration in the study region is dominated by deep convection variability. Winter-time convection is controlled by the stratification of the water column, which in turn depends on upper-layer density variations, all of which are influenced by the wind (Sarafanov, 2009; Delworth et al., 2016; Yashayaev & Loder, 2016, 2017). To further explore the underlying causes of the interannual variability of the DSi inventory, the NAO as an indicator of wind-forcing and the preconditioning variables of temperature, salinity, density, stratification, and heat loss are examined (Fig. B1). In the model, the NAO index was positive between 1988 and 1996 and between 2006 and 2011, with two years of negative NAO in 2009 and 2010. The 5-year running mean indicates that the NAO index started to decline around 1989. According to Brodeau & Koenigk (2016), the 1990s winter-time deep convection shutdown was caused by limited preconditioning of the water column between the warming and the cooling seasons (i.e., autumn-winter). This weak preconditioning is partly induced by a neutral to negative NAO index (Brodeau & Koenigk, 2016), consistent with the model behavior. Associated with the decrease of the NAO index, the model displays a density loss, more stratification, and a warming of the upper layer (Fig. B1). This links the NAO index to the variability of the winter-time deep convection, which is itself linked to the variability of DSi inventory in the model.

On the other hand, variations in Arctic inflow follow variations in the Arctic Oscillation (AO, also referred to as the Northern Annular Mode; Wallace, 2000) index (Kelly et al., 2020; Zhang et al., 2021). We found several similarities when comparing the AO index calculated in the model to the DSi transport through the Northern section. For example, when the index is very positive, as was the case between 1989 and 1993, there is a strong positive DSi transport response compared to the rest of the period considered (i.e., 1980-2015). Following the same logic, when the index was low, from 1985 to 1988, the DSi transport was reduced. The lowest value of DSi transport was found in 2010 which was the year with the lowest AO index. Several studies have converged on the same explanation, which is that accumulation of water in the Beaufort Gyre is reinforced when the atmospheric circulation is anticyclonic, i.e., when the AO index is either negative (Qi et al., 2017; Kelly

https://doi.org/10.5194/egusphere-2023-2538
Preprint. Discussion started: 14 December 2023

et al., 2020; Zhang et al., 2021) or neutral (i.e., close to zero with alternation of weak positive and negative indices; Steele, 2004). In the model, the AO index was strong and positive before 1994, neutral between 1994 and 2006, and tended to be negative after 2006 (Fig 2b). The neutral AO index negatively impacts both volume and DSi transport in the model, which explains the mid-1990s negative trend. The temporal evolution of the volume transport across the Northern section is consistent with the hypothesis of water retention upstream of the Northern section (Fig. C1). However, the slope of DSi transport through the Northern section is much steeper than for volume transport, suggesting a decrease in the DSi concentration of Arctic outflow waters. This difference in slope could be explained by a change in the trajectory of the Arctic waters when the AO index is neutral or negative (Kelly et al., 2019). The Ekman transport generated by the anti-cyclonic atmospheric circulation along the North American coast, drives the current away from the Canadian Arctic Archipelago (CAA; Kelly et al., 2019). This new trajectory crosses a region dominated by the Atlantic inflow (Tremblay et al., 2015; Torrès-Valdès et al., 2013), which is poorer in DSi than Pacific Waters (Scheme and DSi concentration in the Arctic are available in Fig. C2). While the AO index and volume and DSi transport are strongly related up to 1993, and during the period of decline, this relationship is not observed after 2006.

4.3 Implications for future ecosystems

Historically, NAO and AO are correlated (Ambaum et al., 2001; Feldstein & Franzke, 2006; Hamouda et al., 2021), which explains why the variability of Arctic transport is similar to that of deep convection. In future projections, according to the RCP8.5 scenario and two CMIP5 models (MPI-ESM-LR and IPSL-CM5A-LR), it is likely that these two modes of variability will be decorrelated (Hamouda et al., 2021). The intensification of the variability of the pressure dipole over the Pacific, which partly characterizes the AO, contrasting with the weakening of the variability of the NAO and of the pressure dipole over the Arctic, which also characterizes the AO, would be responsible (Hamouda et al., 2021). According to our results, such a change in the climate variability modes implies that the Arctic inflow contribution variability, dependent on the Arctic atmospheric vortex variability (Hatun et al., 2017; Kelly et al., 2019), will be greater than deep convection, modulated by the NAO. Thus, future increases of the Arctic inflow contribution to the DSi inventory variability in the Labrador Sea should be considered.

Whether positive or negative, the NPP anomalies (Fig. 2b) are relatively small compared to local mean values (Fig. 2.a). When integrated over the study area and for the period of DSi decline (1994-2007), NPP exhibits a less significant negative trend than the trend in DSi inventory (-0.06 MgC/yr; p-value < 0.05). This low significance is coherent with NPP trends derived from SeaWiFS (Sea-viewing Wide Field-of-View Sensor) ocean color observations between 1998 and 2007 (Fig. D1). Three (standard-VGPM, Eppley-VGPM, and CAFE models) out of four (CbPM) models for estimating NPP from these observations (https://sites.science.oregonstate.edu/ocean.productivity/) found a negative trend (p-value < 0.05) in the northern/northeastern part of the study region, where NPP is highest for the 1998-2007 period. In the southern half of the region, which includes the convection zone, there has been no consensus on a significant trend among the NPP estimation

https://doi.org/10.5194/egusphere-2023-2538
Preprint. Discussion started: 14 December 2023

models. It can be inferred that the weakening of DSi concentrations in the mid-1990s was not sufficient to significantly impact NPP in the southern Labrador Sea, or that compensatory effects, such as a reduction in light limitation (Harrison & Li, 2008) in response to ML shallowing or a reduction in grazing pressure, might help to maintain NPP levels close to those of 1980-1993.

According to future projections (RCP2.6) the annual maximum MLD of the Labrador Sea could decrease by 10% (for non-abrupt models; Sgubin et al., 2017) compared to the period 2006-2015, or even be restricted to depths to around ten meters for a shutdown of deep convection (Drijfhout et al., 2015). The most extreme projections of changes in winter MLD exceed the range of observed and modeled natural variability of deep convection. The projected reduction in MLD in response to global climate change exceeds that of the 1994-2007 period. It could therefore have a greater impact on DSi availability and NPP, compared to the recent natural analog.

Our results suggest that diatom productivity is modulated by the natural variability of DSi. The signal will spread through the food web, from the dominant mesozooplankton grazer *Calanus finmarchicus,* which represents over 60% of mesozooplankton biomass (Head et al., 2003), to higher trophic levels (Yebra et al., 2009). By forming the base of the food chain, spring bloom dynamics impact the variability of upper trophic levels (Cury et al., 2008) indirectly influencing fish stock variability, independently of fishing practices.

5. Conclusion

The analysis of model output shows that variability of deep winter convection (DWC) was the dominant factor influencing the variability of the DSi inventory in the central Labrador Sea between 1980 and 2015. In turn, DWC responds indirectly to the NAO index, which switched from a positive to a negative phase over the study period, and led to a regime shift in DWC in the mid-1990s. The DWC variability relates to early preconditioning of the water column (e.g., necessary heat loss and destratification) between late autumn and early winter, conditions that are influenced by the North Atlantic Oscillation (NAO). Our results suggest that the regime shift in DWC did not extend to the DSi inventory or the NPP, whose variability also depends on other factors. The variability of DSi transport from the Arctic was correlated with DSi inventory variations, however its quantitative impact is negligible at basin scale (i.e., responsible for only ~3% of the DSi decline in the central Basin). The correlation of the variability was attributed to the correlation between the Arctic Oscillation (AO) with the NAO. We note, however, that the Arctic Inflow contributes more significantly to NPP over the Labrador Shelf, where the model output showed an increase in the nanophytoplankton biomass at the expense of diatoms biomass between 1980 and 2015.

However, North Atlantic natural modes of climate variability (i.e., AO and NAO) are expected to change significantly under climate change and could decorrelate. This decorrelation could increase the contribution of the Arctic inflow to the future Labrador Sea DSi inventory. Moreover, the DWC weakening that is projected under climate change could be more intense than observed during the 1994-2007 period suggesting the possibility for more pronounced impacts on DSi availability and future spring bloom dynamics .

https://doi.org/10.5194/egusphere-2023-2538
Preprint. Discussion started: 14 December 2023

425

Appendices

Appendix A. Transport calculation in the ORCA025 grid

The transport is a product of a velocity in $m.s^{-1}$ and a surface area in m^2. This operation has been done at the model time step (i.e. 900 sec) in the case of the effective transport. It is, therefore, equivalent to a flow rate expressed in Sv (= 10^6 $m^3.s^{-1}$).

430 Transport calculation depends on the direction of the section's integration on the model grid (represented by the red arrow in Fig. A1). The sum of horizontal (Fig. A1) and vertical transport components gives the flux balance across the section resulting in the net volume transport. The ORCA025 grid is irregular and follows the Arakawa's grid C shift between (i) U and V points, relative to the velocities and effective transport components; (ii) T point for computation of DSi concentration, temperature, and salinity; and (iii) F point is relative to vorticities (not represented in Fig. AA). The DSi
435 transport is the integration along the section of the effective volume transport at point U or V and average DSi concentration. According to Fig. A1, DSi transport across the section at the point T(j,i) is the product of the average DSi concentration of the T point surrounding the V(j,i) point, i.e. of the point T(j,i) and T(j+1,i).

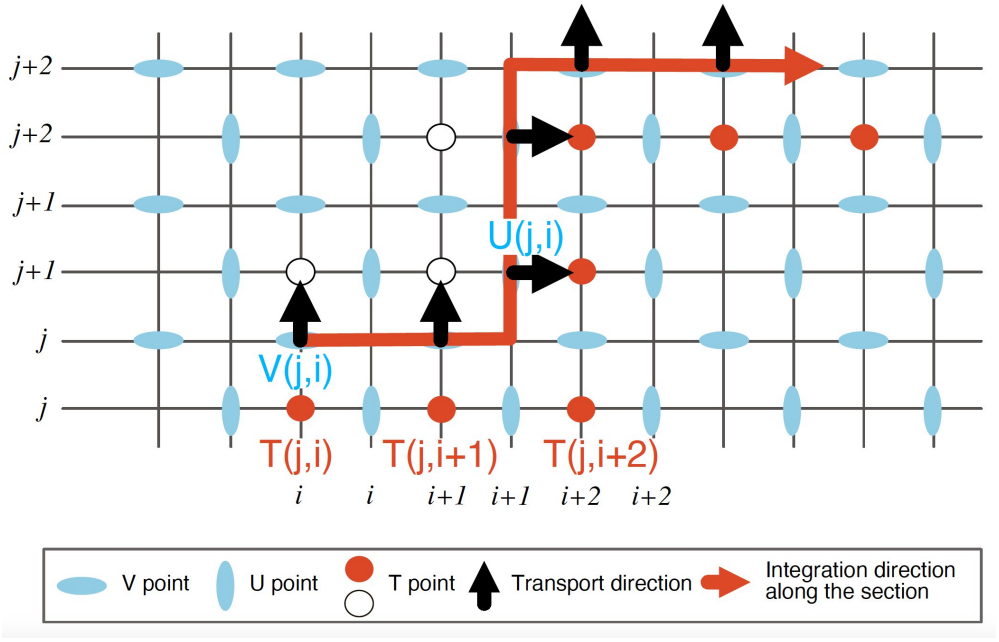

Figure A1. Schematic of the ORCA025 grid adapted from Madec et al., (2017) highlighting points used to calculate
440 **volume and DSi transport across a section.** Orientation of black arrows are conditioned by model convention (positive sign for northward and eastward transport and velocities).

Appendix B. Heat Content and Stratification Index (1980-2015)

https://doi.org/10.5194/egusphere-2023-2538
Preprint. Discussion started: 14 December 2023

To evaluate the preconditioning of deep winter convection (November-December) over the entire period (1980-2015) and in the upper layer (< 450 m), the heat content (HC) was calculated following Eq. (B1).

$$HC\,(x, y, h) = \sigma_0\,(x, y) \times Cp\ (x, y) \int_0^{h=450m} T\ (x, y, z)\, dz \qquad \text{(B1)}$$

where σ_0 is the mean potential density of the upper layer equal to 1027 kg.m^{-3}, Cp is the specific heat capacity, equal to 3990 J.kg^{-1}.K^{-1}. Both are calculated with the Gibbs Sea Water Oceanographic Toolbox (Feistel, 2003; 2008) from absolute salinity, conservative temperature and pressure. T is the potential temperature in K. The heat content, HC, is given in J.m^{-2}.

To further characterize the preconditioning of the upper layer, we calculated a Stratification Index (SI) representative of December in each year (Beuvier et al., 2010; Keller et al., 2021; Léger et al., 2016) following Eq (B2).

$$SI\ (x, y, h) = \int_0^{h=450m} N^2\ (x, y, z)\ z\, dz \qquad \text{(B2)}$$

where N^2 is the Brunt-Väisälä frequency $N^2 = \frac{g}{\sigma_0} \frac{\partial \sigma}{\partial z}$ with g the acceleration due to gravity (g = 9.81 m.s^{-2}) and σ_0 the potential density at each grid cell in kg.m^{-3}. SI corresponds to the buoyancy that must be removed to allow the water column to be mixed to a depth of 450 m. Following Keller et al. (2021), the Brunt-Väisälä frequency is approximated constant over the 0 and 450 m depth interval, which leads to the simplified equation: $SI\ (x, y, h) = \frac{h^2}{2} N^2\,(x, y)$, where h equals 450 m.

https://doi.org/10.5194/egusphere-2023-2538
Preprint. Discussion started: 14 December 2023

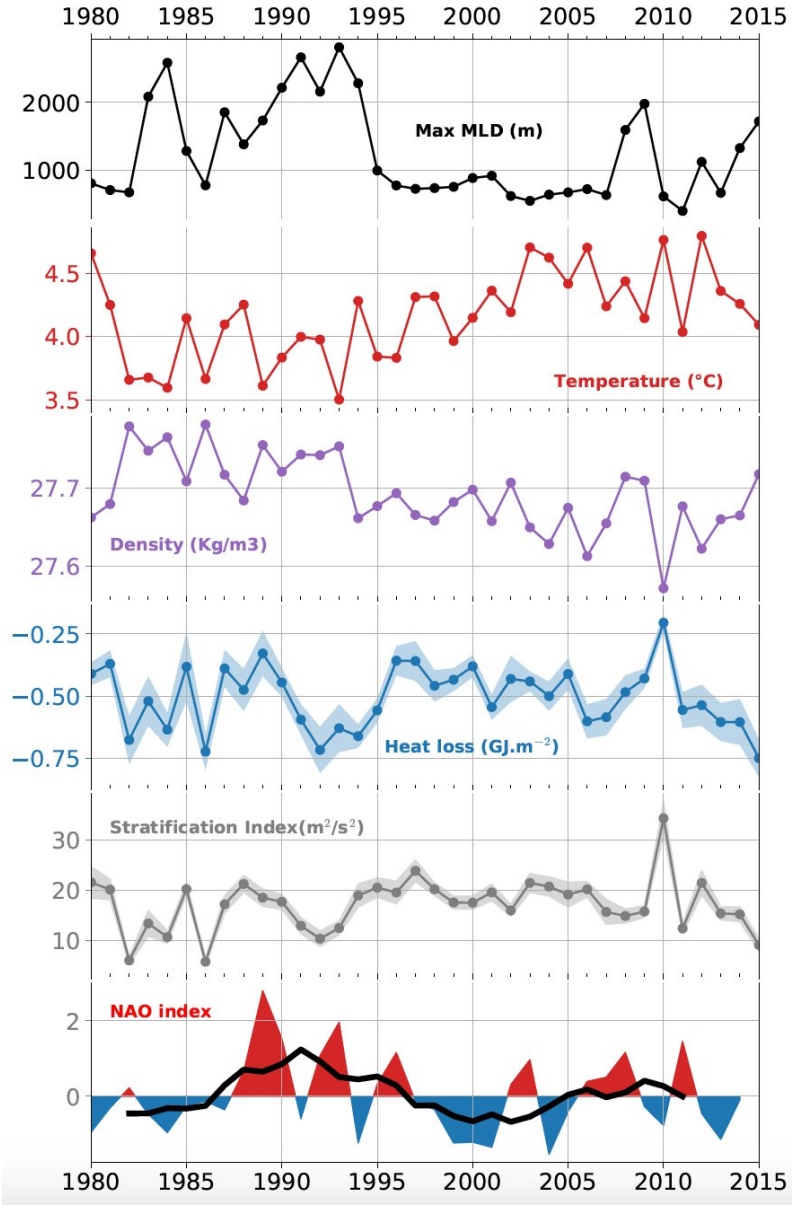

Figure B1. Temporal evolution of the upper layer preconditioning for the period 1980-2015. (black) Annual Maximum MLD over the study area. (red) Average temperature and potential density (in purple) within the 1980-2015 average convection area in November (i.e. time of year when the sign of the average upper layer temperature anomalies changes from positive to negative). (blue) Heat loss as defined by the difference of heat content between November and December (surrounding transition from the warming to cooling season) over the 1980-2015 period. (gray) Stratification index in December, i.e at the beginning of the cooling season. The last panel displays the winter-time NAO index. The red line

https://doi.org/10.5194/egusphere-2023-2538
Preprint. Discussion started: 14 December 2023

exhibits the 5-year running mean of the index. All of the colored shadings around mean values, except for the NAO, represent standard deviations.

Appendix C. Arctic Inflow

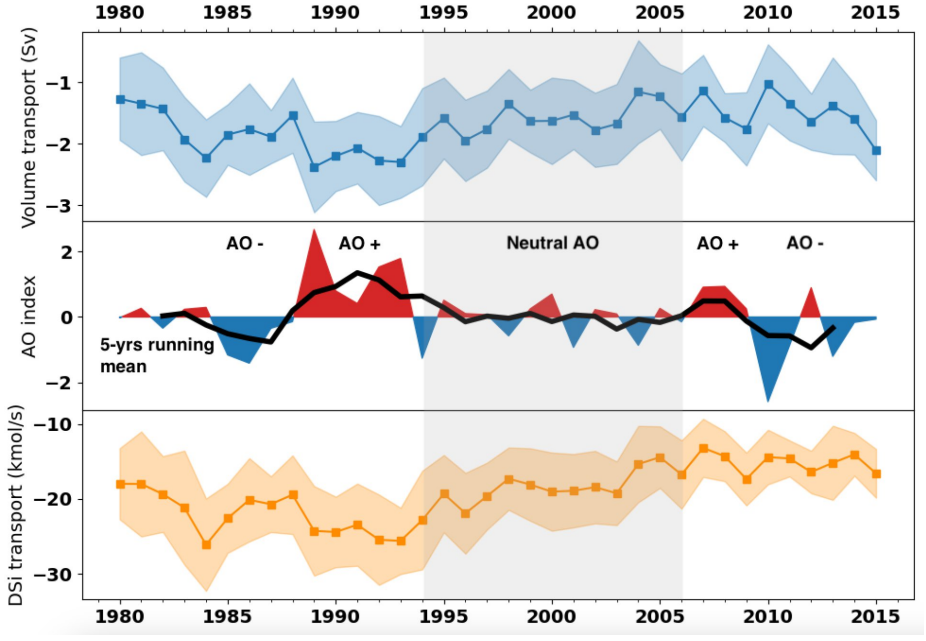

Figure C1. Annual average of the net volume transport, Arctic Oscillation index, and DSi transport across the northern boundary. Coloured shading shows the standard deviation around the annual mean. The AO index has been calculated for the winter months (DJF). The solid black line over the AO index is the 5-year running mean. The gray shaded area highlights years when the AO index was neutral. Note that transport is weaker as it approaches zero.

https://doi.org/10.5194/egusphere-2023-2538
Preprint. Discussion started: 14 December 2023

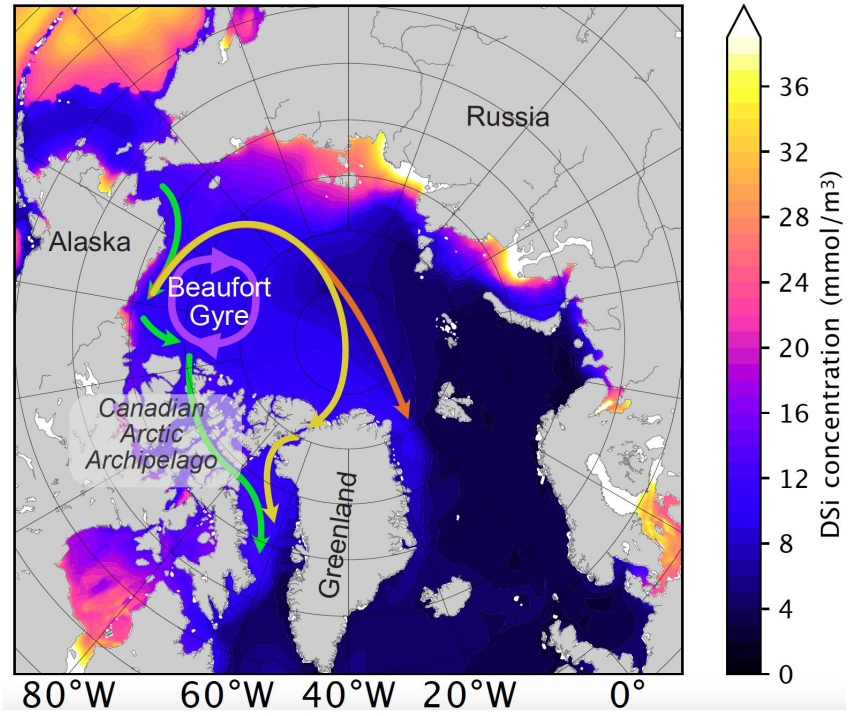

Figure C2. Annual upper 450 m average DSi concentration in the Arctic Ocean for the period preceding the DSi decline (1980-1993). The concentration diagrams show the trajectories according to Kelly et al. (2020). The green arrow illustrates the dominant trajectory of water masses under AO+ conditions (i.e., cyclonic atmospheric circulation). The orange and yellow routes show the deviation during the AO- conditions (i.e., anti-cyclonic atmospheric circulation)

Appendix D. Observed Net Primary Production

https://doi.org/10.5194/egusphere-2023-2538
Preprint. Discussion started: 14 December 2023

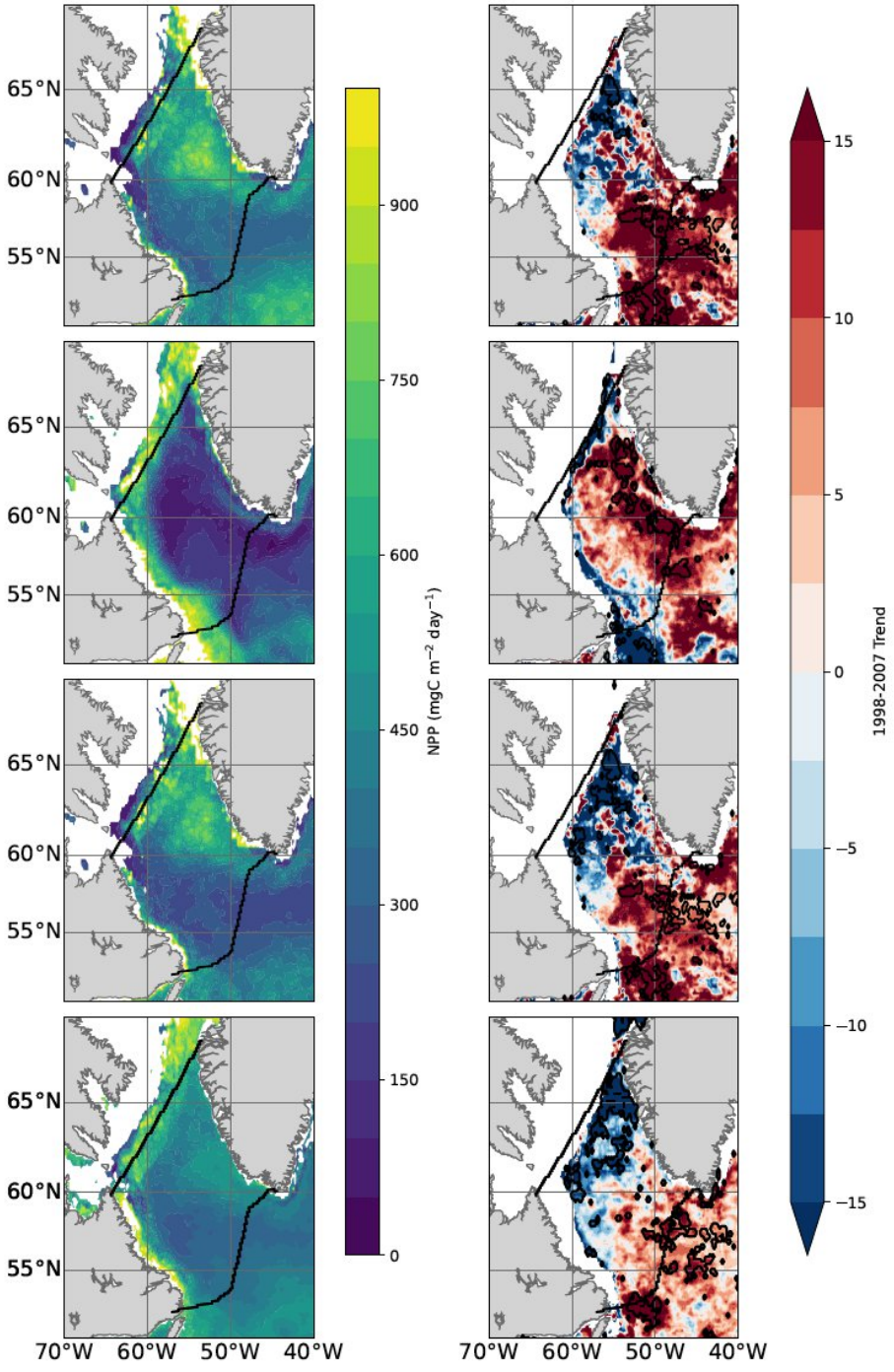

Figure D1. Mean and trends of 1998-2007 NPP integrated from top to bottom and from April to June (i.e., spring bloom). NPP is estimated from SEAWiFs ocean color using the standard VGPM model, (c-d) the CbPM model, (e-f) the Eppley derived-VGPM model which considers temperature dependence of phytoplankton growth, based on the work of

https://doi.org/10.5194/egusphere-2023-2538
Preprint. Discussion started: 14 December 2023

Eppley et al. (1972), and (g-h) the CAFE model. In b, d, f, and h, significant trends (p-value $<$ 0.05) are circled in black. NPP trends could not be calculated over the entire period of this study (1994-2007) due to a lack of observations prior to 1998.

505

Supplementary material and data availability

Model output used in this study is available from the IPSL Data Catalog via the DOI: https://doi.org/10.14768/99d68638-53d3-49b6-9af4-c19f21670a8e.

Evaluation of model output for the Labrador Sea are available in the Supplementary material file.

510

Author contributions

A.Dale: Conceptualization, Methodology, Formal Analysis, Investigation, Visualization, Writing - Original Draft

M. Gehlen: Conceptualization, Investigation, Writing - Original Draft, Supervision, Funding Acquisition

D. Wallace: Conceptualization, Investigation, Writing - Original Draft, Supervision, Funding Acquisition

515 G. Bénard: Formal Analysis

C. Éthé: Software, Resources

E. Aleeksenko: Software, Resources

Competing interests

520 The authors declare that they have no conflict of interest.

Acknowledgments

The NEMO-PISCES simulation was carried out with resources from TGCC and IDRIS through a GENCI/DARI grant (gen0040). A.D. was funded by a MESRI doctoral research fellowship and received partial support from a French Canada 525 Research Fund grant. MG acknowledges funding from the European Union's Horizon 2020 research and innovation programme under grant agreement number 862923 (project AtlantECO) and grant agreement number 820989 (project COMFORT). The work was funded partially by the Ocean Frontier Institute (Module B) and by a grant of the France Canada Research Fund to Katja Fennel and Marion Gehlen. We are grateful to Louis Petiteau for his participation in the model evaluation and to Lorenza Raimondi for providing interpolated DSi concentration along the AR7W section. We want to 530 acknowledge Gilles Reverdin, James Orr, and Kitty Kam for constructive discussions and comments.

References

https://doi.org/10.5194/egusphere-2023-2538
Preprint. Discussion started: 14 December 2023

Aksenov, Y., Karcher, M., Proshutinsky, A., Gerdes, R., Cuevas, B. de, Golubeva, E., Kauker, F., Nguyen, A. T., Platov, G. A., Wadley, M., Watanabe, E., Coward, A. C., & Nurser, A. J. G. (2016). Arctic pathways of Pacific Water : Arctic Ocean Model Intercomparison experiments. *Journal of Geophysical Research: Oceans*, *121*(1), 27-59. https://doi.org/10.1002/2015JC011299

Ambaum, M. H. P., Hoskins, B. J., & Stephenson, D. B. (2001). Arctic Oscillation or North Atlantic Oscillation? *Journal of Climate*, *14*(16), 3495-3507. https://doi.org/10.1175/1520-0442(2001)014<3495:AOONAO>2.0.CO;2

Aumont, O., Ethé, C., Tagliabue, A., Bopp, L., & Gehlen, M. (2015). PISCES-v2 : An ocean biogeochemical model for carbon and ecosystem studies. *Geoscientific Model Development*, *8*(8), 2465-2513. https://doi.org/10.5194/gmd-8-2465-2015

Bersch, M., Yashayaev, I., & Koltermann, K. P. (2007). Recent changes of the thermohaline circulation in the subpolar North Atlantic. Ocean Dynamics, 57, 223-235.

Beuvier, J., Sevault, F., Herrmann, M., Kontoyiannis, H., Ludwig, W., Rixen, M., ... & Somot, S. (2010). Modeling the Mediterranean Sea interannual variability during 1961–2000: focus on the Eastern Mediterranean Transient. *Journal of Geophysical Research: Oceans*, *115*(C8).

Brodeau, L., & Koenigk, T. (2016). Extinction of the northern oceanic deep convection in an ensemble of climate model simulations of the 20th and 21st centuries. *Climate Dynamics*, *46*(9-10), 2863-2882. https://doi.org/10.1007/s00382-015-2736-5

Conti, L., & Scardi, M. (2010). Fisheries yield and primary productivity in large marine ecosystems. *Marine Ecology Progress Series*, *410*, 233-244. https://doi.org/10.3354/meps08630

Delworth, T. L., Zeng, F., Vecchi, G. A., Yang, X., Zhang, L., & Zhang, R. (2016). The North Atlantic Oscillation as a driver of rapid climate change in the Northern Hemisphere. *Nature Geoscience*, *9*(7), 509-512. https://doi.org/10.1038/ngeo2738

Drijfhout, S., Bathiany, S., Beaulieu, C., Brovkin, V., Claussen, M., Huntingford, C., Scheffer, M., Sgubin, G., & Swingedouw, D. (2015). Catalogue of abrupt shifts in Intergovernmental Panel on Climate Change climate models. *Proceedings of the National Academy of Sciences*, *112*(43). https://doi.org/10.1073/pnas.1511451112

Dussin, R., Barnier, B., Brodeau, L., & Molines, J.-M. (2016). *Drakkar forcing set DFS5*. https://www.drakkar-ocean.eu/publications/reports/report_DFS5v3_April2016.pdf

Egge, J., & Aksnes, D. (1992). Silicate as regulating nutrient in phytoplankton competition. *Marine Ecology Progress Series*, *83*, 281-289. https://doi.org/10.3354/meps083281

Eppley, R. W. (1972). Temperature and phytoplankton growth in the sea. *Fish. bull*, *70*(4), 1063-1085.

Feistel, R. (2003). A new extended Gibbs thermodynamic potential of seawater. *Progress in Oceanography*, *58*(1), 43-114.

Feistel, R. (2008). A Gibbs function for seawater thermodynamics for− 6 to 80 C and salinity up to 120 g kg–1. *Deep Sea Research Part I: Oceanographic Research Papers*, *55*(12), 1639-1671.

https://doi.org/10.5194/egusphere-2023-2538
Preprint. Discussion started: 14 December 2023

Feldstein, S. B., & Franzke, C. (2006). Are the North Atlantic Oscillation and the Northern Annular Mode Distinguishable? *Journal of the Atmospheric Sciences*, *63*(11), 2915-2930. https://doi.org/10.1175/JAS3798.1

Fragoso, G. M., Poulton, A. J., Yashayaev, I. M., Head, E. J. H., Stinchcombe, M. C., & Purdie, D. A. (2016). Biogeographical patterns and environmental controls of phytoplankton communities from contrasting hydrographical zones of the Labrador Sea. *Progress in Oceanography*, *141*, 212-226. https://doi.org/10.1016/j.pocean.2015.12.007

Glen Harrison, W., Yngve Børsheim, K., Li, W. K. W., Maillet, G. L., Pepin, P., Sakshaug, E., Skogen, M. D., & Yeats, P. A. (2013). Phytoplankton production and growth regulation in the Subarctic North Atlantic : A comparative study of the Labrador Sea-Labrador/Newfoundland shelves and Barents/Norwegian/Greenland seas and shelves. *Progress in Oceanography*, *114*, 26-45. https://doi.org/10.1016/j.pocean.2013.05.003

Hakkinen, S. (2004). Decline of Subpolar North Atlantic Circulation During the 1990s. *Science*, *304*(5670), 555-559. https://doi.org/10.1126/science.1094917

Häkkinen, S., Rhines, P. B., & Worthen, D. L. (2011). Atmospheric blocking and Atlantic multidecadal ocean variability. *Science*, *334*(6056), 655-659.

Hamouda, M. E., Pasquero, C., & Tziperman, E. (2021). Decoupling of the Arctic Oscillation and North Atlantic Oscillation in a warmer climate. *Nature Climate Change*, *11*(2), 137-142. https://doi.org/10.1038/s41558-020-00966-8

Harrison, W., & Li, W. (2008). Phytoplankton growth and regulation in the Labrador Sea : Light and nutrient limitation. *Journal of Northwest Atlantic Fishery Science*, *39*, 71-82. https://doi.org/10.2960/J.v39.m592

Hatun, H. (2005). Influence of the Atlantic Subpolar Gyre on the Thermohaline Circulation. *Science*, *309*(5742), 1841-1844. https://doi.org/10.1126/science.1114777

Hátún, H., Azetsu-Scott, K., Somavilla, R., Rey, F., Johnson, C., Mathis, M., Mikolajewicz, U., Coupel, P., Tremblay, J.-É., Hartman, S., Pacariz, S. V., Salter, I., & Ólafsson, J. (2017). The subpolar gyre regulates silicate concentrations in the North Atlantic. *Scientific Reports*, *7*(1), 14576. https://doi.org/10.1038/s41598-017-14837-4

Head, E. J. H., Harris, L. R., & Yashayaev, I. (2003). Distributions of Calanus spp. And other mesozooplankton in the Labrador Sea in relation to hydrography in spring and summer (1995–2000). *Progress in Oceanography*, *59*(1), 1-30. https://doi.org/10.1016/S0079-6611(03)00111-3

Hurrell, J. W., Kushnir, Y., Ottersen, G., & Visbeck, M. (2003). An overview of the North Atlantic oscillation. Geophysical Monograph-American Geophysical Union, 134, 1-36.

Kelly, S. J., Popova, E., Aksenov, Y., Marsh, R., & Yool, A. (2020). They Came From the Pacific : How Changing Arctic Currents Could Contribute to an Ecological Regime Shift in the Atlantic Ocean. *Earth's Future*, *8*(4). https://doi.org/10.1029/2019EF001394

Keller, D., Givon, Y., Pennel, R., Raveh-Rubin, S., & Drobinski, P. J. (2022). Untangling the Mistral and Seasonal Atmospheric Forcing Driving Deep Convection in the Gulf of Lion: 1993-2013. *Authorea Preprints*.

https://doi.org/10.5194/egusphere-2023-2538
Preprint. Discussion started: 14 December 2023

Lazier, J., Hendry, R., Clarke, A., Yashayaev, I., & Rhines, P. (2002). Convection and restratification in the Labrador Sea, 1990–2000. *Deep Sea Research Part I: Oceanographic Research Papers*, *49*(10), 1819-1835. https://doi.org/10.1016/S0967-0637(02)00064-X

Léger, F., Lebeaupin Brossier, C., Giordani, H., Arsouze, T., Beuvier, J., Bouin, M. N., ... & Nuret, M. (2016). Dense water formation in the north-western Mediterranean area during HyMeX-SOP2 in 1/36° ocean simulations: Sensitivity to initial conditions. *Journal of Geophysical Research: Oceans*, *121*(8), 5549-5569.

Lenton, T. M., Held, H., Kriegler, E., Hall, J. W., Lucht, W., Rahmstorf, S., & Schellnhuber, H. J. (2008). Tipping elements in the Earth's climate system. *Proceedings of the National Academy of Sciences*, *105*(6), 1786-1793. https://doi.org/10.1073/pnas.0705414105

Lohmann, K., Drange, H., & Bentsen, M. (2009). Response of the North Atlantic subpolar gyre to persistent North Atlantic oscillation like forcing. *Climate dynamics*, *32*, 273-285.

Madec, G., Bourdallé-Badie, R., Bouttier, P.-A., Bricaud, C., Bruciaferri, D., Calvert, D., Chanut, J., Clementi, E., Coward, A., & Delrosso, D. (2017). *NEMO ocean engine*. 412.

McKay, D. I. A., Staal, A., Abrams, J. F., Winkelmann, R., Sakschewski, B., Loriani, S., Fetzer, I., Cornell, S. E., Rockström, J., & Lenton, T. M. (2022). Exceeding 1.5°C global warming could trigger multiple climate tipping points. *CLIMATE CHANGE*, 12.

McKinley, G. A., Ritzer, A. L., & Lovenduski, N. S. (2018). Mechanisms of northern North Atlantic biomass variability. *Biogeosciences*, *15*(20), 6049-6066. https://doi.org/10.5194/bg-15-6049-2018

Nelson, D., & Dortch, Q. (1996). Silicic acid depletion and silicon limitation in the plume of the Mississippi River:evidence from kinetic studies in spring and summer. *Marine Ecology Progress Series*, *136*, 163-178. https://doi.org/10.3354/meps136163

Qi, D., Chen, L., Chen, B., Gao, Z., Zhong, W., Feely, R. A., Anderson, L. G., Sun, H., Chen, J., Chen, M., Zhan, L., Zhang, Y., & Cai, W.-J. (2017). Increase in acidifying water in the western Arctic Ocean. *Nature Climate Change*, *7*(3), 195-199. https://doi.org/10.1038/nclimate3228

Raimondi, L., Tanhua, T., Azetsu-Scott, K., Yashayaev, I., & Wallace, D. W. R. (2021). A 30 -Year Time Series of Transient Tracer-Based Estimates of Anthropogenic Carbon in the Central Labrador Sea. *Journal of Geophysical Research: Oceans*, *126*(5). https://doi.org/10.1029/2020JC017092

Rousseaux, C., & Gregg, W. (2013). Interannual Variation in Phytoplankton Primary Production at A Global Scale. *Remote Sensing*, *6*(1), 1-19. https://doi.org/10.3390/rs6010001

Rühs, S., Oliver, E. C. J., Biastoch, A., Böning, C. W., Dowd, M., Getzlaff, K., Martin, T., & Myers, P. G. (2021). Changing Spatial Patterns of Deep Convection in the Subpolar North Atlantic. *Journal of Geophysical Research: Oceans*, *126*(7), e2021JC017245. https://doi.org/10.1029/2021JC017245

https://doi.org/10.5194/egusphere-2023-2538
Preprint. Discussion started: 14 December 2023

Sarafanov, A. (2009). On the effect of the North Atlantic Oscillation on temperature and salinity of the subpolar North Atlantic intermediate and deep waters. *ICES Journal of Marine Science*, *66*(7), 1448-1454. https://doi.org/10.1093/icesjms/fsp094

Sgubin, G., Swingedouw, D., Drijfhout, S., Mary, Y., & Bennabi, A. (2017). Abrupt cooling over the North Atlantic in modern climate models. *Nature Communications*, *8*(1), 14375. https://doi.org/10.1038/ncomms14375

Steele, M. (2004). Circulation of summer Pacific halocline water in the Arctic Ocean. *Journal of Geophysical Research*, *109*(C2), C02027. https://doi.org/10.1029/2003JC002009

Stock, C. A., John, J. G., Rykaczewski, R. R., Asch, R. G., Cheung, W. W. L., Dunne, J. P., Friedland, K. D., Lam, V. W. Y., Sarmiento, J. L., & Watson, R. A. (2017). Reconciling fisheries catch and ocean productivity. *Proceedings of the National Academy of Sciences*, *114*(8). https://doi.org/10.1073/pnas.1610238114

Swingedouw, D. (2022). *AMOC Recent and Future Trends : A Crucial Role for Oceanic Resolution and Greenland Melting? 4*, 21.

Tesdal, J.-E., Ducklow, H. W., Goes, J. I., & Yashayaev, I. (2022). Recent nutrient enrichment and high biological productivity in the Labrador Sea is tied to enhanced winter convection. *Progress in Oceanography*, *206*, 102848. https://doi.org/10.1016/j.pocean.2022.102848

Thompson, D. W., & Wallace, J. M. (1998). The Arctic Oscillation signature in the wintertime geopotential height and temperature fields. *Geophysical research letters*, *25*(9), 1297-1300.

Torres-Valdés, S., Tsubouchi, T., Bacon, S., Naveira-Garabato, A. C., Sanders, R., McLaughlin, F. A., Petrie, B., Kattner, G., Azetsu-Scott, K., & Whitledge, T. E. (2013). Export of nutrients from the Arctic Ocean : ARCTIC OCEAN NUTRIENT EXPORTS. *Journal of Geophysical Research: Oceans*, *118*(4), 1625-1644. https://doi.org/10.1002/jgrc.20063

Tremblay, J.-É. (2002). Impact of the large-scale Arctic circulation and the North Water Polynya on nutrient inventories in Baffin Bay. *Journal of Geophysical Research*, *107*(C8), 3112. https://doi.org/10.1029/2000JC000595

Tremblay, J. É., Anderson, L. G., Matrai, P., Coupel, P., Bélanger, S., Michel, C., & Reigstad, M. (2015). Global and regional drivers of nutrient supply, primary production and CO2 drawdown in the changing Arctic Ocean. *Progress in Oceanography*, *139*, 171-196.

Vancoppenolle, M., Fichefet, T., Goosse, H., Bouillon, S., Madec, G., & Maqueda, M. A. M. (2009). Simulating the mass balance and salinity of Arctic and Antarctic sea ice. 1. Model description and validation. *Ocean Modelling*, *27*(1-2), 33-53. https://doi.org/10.1016/j.ocemod.2008.10.005

Wallace, J. M. (2000). North Atlantic Oscillation/annular mode : Two paradigms-one phenomenon. *Quarterly Journal of the Royal Meteorological Society*, *126*(564), 791-805. https://doi.org/10.1256/smsqj.56401

Yashayaev, I. (2023). *The Labrador Sea sets a new reference point in the subpolar North Atlantic climate record* [Preprint]. In Review. https://doi.org/10.21203/rs.3.rs-2663705/v1

https://doi.org/10.5194/egusphere-2023-2538
Preprint. Discussion started: 14 December 2023

Yashayaev, I., & Loder, J. W. (2016). Recurrent replenishment of Labrador Sea Water and associated decadal-scale variability : 2015 Convection in Labrador Sea. *Journal of Geophysical Research: Oceans*, *121*(11), 8095-8114. https://doi.org/10.1002/2016JC012046

Yashayaev, I., & Loder, J. W. (2017). Further intensification of deep convection in the Labrador Sea in 2016. *Geophysical Research Letters*, *44*(3), 1429-1438. https://doi.org/10.1002/2016GL071668

Yeats, P., Ryan, S., & Harrison, G. (2011). Temporal Trends in Nutrient and Oxygen Concentrations in the Labrador Sea and on the Scotian Shelf. *Journal of Geophysical Research*, *111*(C6), C06022. https://doi.org/10.1029/2005JC003159

Yebra, L., Harris, R. P., Head, E. J. H., Yashayaev, I., Harris, L. R., & Hirst, A. G. (2009). Mesoscale physical variability affects zooplankton production in the Labrador Sea. *Deep Sea Research Part I: Oceanographic Research Papers*, *56*(5), 703-715. https://doi.org/10.1016/j.dsr.2008.11.008

Zhang, J., Weijer, W., Steele, M., Cheng, W., Verma, T., & Veneziani, M. (2021). Labrador Sea freshening linked to Beaufort Gyre freshwater release. *Nature Communications*, *12*(1), 1229. https://doi.org/10.1038/s41467-021-21470-3